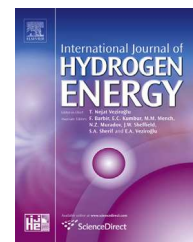


Available online at www.sciencedirect.com

ScienceDirect

journal homepage: www.elsevier.com/locate/he

Atom probe tomography observation of hydrogen in high-Mn steel and silver charged via an electrolytic route

D. Haley^{*}, S.V. Merzlikin, P. Choi, D. Raabe

Max-Planck-Institut für Eisenforschung, Max-Planck-Straße 1, D-40237 Düsseldorf, Germany

ARTICLE INFO

Article history:

Received 11 March 2014

Received in revised form

21 May 2014

Accepted 26 May 2014

Available online 2 July 2014

Keywords:

Atom probe

High-Mn steel

Electrolytic charging

ABSTRACT

We investigate an electrolytic route for hydrogen charging of metals and its detection in Atom Probe Tomography (APT) experiments. We charge an austenitic Fe-30Mn-8Al-1.2C (wt.%) weight reduced high-Mn steel and subsequently demonstrate the detectability of deuterium in an APT experiment. The experiment is repeated with a deposited Ag film upon an APT tip of a high-Mn steel. It is shown that a detectable deuterium signal can be seen in the high-Mn steel, and a D:H ratio of 0.84 can be reached in Ag films. Additionally, it was found that the predicted time constraint on detectability of D in APT was found to be lower than predicted by bulk diffusion for the high-Mn steel.

Copyright © 2014, Hydrogen Energy Publications, LLC. Published by Elsevier Ltd. All rights reserved.

Introduction and motivation

The fundamental driving force for hydrogen-related materials research is the embrittling nature of hydrogen, whether originating from a gaseous molecular form, or from hydrogen containing liquids [1]. As a species in operating environments, hydrogen is near-ubiquitous. Austenitic steels, such as Al-containing Mn-stabilised steels, have been proposed as an alternative material for environments where hydrogen embrittlement may be problematic [2,3]. Al-enriched material has been demonstrated to have a higher embrittlement resistance than Al-free materials [4], which has been attributed to modification of stacking fault energies [5], surface oxide formation, stress reduction or change in shear modulus. The exact mechanism is, however, the subject of ongoing discussion [6].

In order to gain an understanding of the hydrogen embrittling mechanism and thus allow for improved

microstructural design, further direct characterisation of the interaction between hydrogen and the microstructure is desirable. A greater microstructural knowledge, and thus design capability, would allow for enhancing the ductility and toughness of these materials in the presence of hydrogen [7].

Localisation of hydrogen at the nanostructural level is a complex nano-analysis task, with few methods able to simultaneously localise the position of hydrogen and quantify its concentration. Indeed, much knowledge about hydrogen in the context of engineering materials has been garnered from either simulation or bulk testing. Such applicable techniques include thermal desorption spectroscopy [8], computational methods such as quantum-mechanical calculations [9], or more recently, micro-scale scanning methods that measure hydrogen absorption into a hydride forming layer via tip-scanning [10].

For interpreting integrative experimental results, such as thermal desorption, or validating theoretical predictions of

^{*} Corresponding author. Tel.: +49 (0) 211 67 92 152.

E-mail address: d.haley@mpie.de (D. Haley).

<http://dx.doi.org/10.1016/j.ijhydene.2014.05.169>

0360-3199/Copyright © 2014, Hydrogen Energy Publications, LLC. Published by Elsevier Ltd. All rights reserved.

hydrogen trapping and embrittlement mechanisms a better knowledge of the actual position of hydrogen in the affected microstructure is required. Hence, in this work we develop an approach to charge metals with hydrogen and map it subsequently by using Atom Probe Tomography (APT).

Hydrogen detection in APT has been conducted previously by several authors [11–15], by modification of their APT systems to accept gaseous deuterium. However, this route has several limitations. Firstly, the method requires the modification of an APT instrument from current commercial configurations [16] to obtain spatially resolvable signals, and the second limitation is the achievable loading fugacities. An alternative method for introducing deuterium into a sample was investigated by Takamizawa [15], whereby deuterium was implanted by ion beam methods. One of the more curious applications for deuterium charged APT-like samples is in experimental compact neutron generators [39], where very high deuterium evaporation rates were observed.

As hydrogen is largely considered a difficult to remove contaminating species in APT designs, systems are not usually configured to allow deliberate introduction of such gases into the vacuum system, making gaseous introduction impractical for many APT systems. Secondly, the theoretically achievable fugacities using electrolytic charging are several orders of magnitude higher than are achievable with a low-pressure gas charging apparatus [17], and thus significantly higher hydrogen concentrations should be able to be introduced into samples. Realisable concentrations can (with sufficiently fast quenching) be up to 0.5 (at. H)/(metal atom) [17]. With higher hydrogen concentrations, the ability for APT systems to detect deuterium segregation should be commensurately improved, yielding a higher signal-to-noise ratio.

With the objective of investigating the practicality and limitations of hydrogen measurement in APT when introduced via an electrolytic pathway, we investigate deuterium detection by APT within austenitic Fe–Mn materials.

Current experimental results on H and D trapping in APT

Deep trapping of hydrogen at energetically favourable lattice defect positions is a well-known mechanism for hydrogen entrapment within materials, for which several theoretical models exist [18]. These models, used to explain bulk measurements [19], predict the trapping of hydrogen to specific microstructural features within the bulk material. Possible trapping sites could include grain boundaries [20], dislocation cores [21], nanovoids [22], or point-defects such as vacancies [23]. However, to date, the capacity for direct real-space imaging of hydrogen has been limited, in part due to difficulties in characterisation of light elements by microscopic means [24]. Direct imaging of hydrogen at microstructural features would enable improved alloy design to minimise embrittlement effects [25].

For hydrogen imaging, in particular for understanding interactions between hydrogen and microstructural features, APT is a highly promising technique. The works of Takahashi, Gemma and Takamizawa demonstrate that imaging can be

performed for sufficiently high D-content within materials. The highest observable D:H ratios with a visible 3D distribution are reported by Gemma for VH (D:H $\gg 1$) [13], by Takahashi for VC (D:H ~ 0.5) [12] and TiC (D:H ~ 0.066) [11], and finally Takamizawa in D-implanted Si wafers with a value of 0.04 (D:H – H₂:H)¹ [15]. Karesky reports a D:H ratio of ~ 0.2 for a 316 stainless steel, but no 3D distribution is given [14].

In this work, this ratio is used as the primary measurement of hydrogen signal quality within the material. The absolute magnitude of the mass = 2 peak is a weaker metric than the ratio measure, D:H, for the effectiveness of hydrogen localisation, due to the non-negligible probability of ionisation of an H₂⁺ molecule, which overlaps with the D⁺ peak. Having a large ratio allows for determining if a fluctuation in the mass = 2 peak is simply a reflection of increased H generation due to local specimen chemistry or surface crystallography, particularly important when examining low total D concentrations.

For experiments with a high unloaded H₂⁺ peak amplitude, this background should be subtracted from mass spectra of deuterium loaded samples. This is particularly important for laser assisted APT experiments, due to the increased molecular ion formation associated with laser experiments [26]. Furthermore, it may be that the absolute H levels may vary with the presence of features in the dataset, which could give the appearance of deuterium at microstructural features if only observing D counts, rather than a localised ratio.

Deuterium was considered an appropriate substitute for hydrogen investigations, as necessitated by the omnipresent H background. However, it is hypothetically possible that there is a different partitioning of deuterium than for hydrogen to trapping locations. From a practical perspective this seems unlikely, as the most selective reactions for deuterium enrichment (i.e. the Girdler-Sulfide process for heavy water enrichment), have D:H separation coefficients of approximately 2.3 [27]. This implies that, at equilibrium, each hydrogen atom at a binding location is accompanied by 2.3 deuterium atoms for this reaction. It is unlikely that trapping in steel samples would exceed this selectivity by orders of magnitude, and lead to different binding sites for D and H, and such a result would be highly interesting in and of itself as a candidate for heavy water enrichment. Obtaining such a result seems unlikely, given the scope of this study.

Thus, this work aims to investigate electrochemical deuterium loading as a route for maximising the observable deuterium content in APT experiments. This approach opens new possibilities for APT experiments in two ways. Firstly, the increased signal allows for better detectability for hydrogen, particularly to potential trapping defects, and secondly, the method simplifies the experimental requirements for H charging and detection, making this method available to almost any APT system. Specifically, we load high-Mn austenitic steels and demonstrate that electrochemical loading does successfully introduce detectable quantities of deuterium into these samples.

¹ H₂:H ratio from uncharged specimen, D:H from charged specimen.

Experimental method

A customised electrochemical cell for performing hydrogen charging from the liquid phase was developed, in order to allow hydrogen to be injected into an APT tip (Fig. 1). Experiments were performed under an Ar atmosphere, with solution contacting components of borosilicate glass, gold, Teflon or platinum manufacture, and additionally a NAFION membrane isolating the electrode in order to avoid contamination from cell dissolution and re-deposition. Charging was performed at room temperature. Current-time curves are not reproduced here, owing to the limited size of the material ($\sim 1 \mu\text{m} \times 500 \text{ nm} \times 500 \text{ nm}$), as compared to the holder itself, thus obscuring any useful current-time data.

The APT experiments were conducted using a LEAP 3000X HR system. APT runs were undertaken using voltage mode pulsing at a pulse fraction of 0.15, a base temperature of 70 K, and an evaporation rate of 0.5, with a pulse frequency of 100 kHz. Deuterium loading was conducted using a 0.1 M NaOD in D_2O solution for 1 h at -1.2 V .

The experiment was conducted in the following manner: First a FIB prepared tip (2 kV final mill) was manufactured, by placing it on a silicon TEM-grid mount (Fig. 2). FIB prepared samples allowed for more rapid transfer as all specimens could be mounted onto a single holder, reducing the time required for specimen transfer after charging, whilst simultaneously allowing for multiple sample charging. Once

charged, the sample was loaded into the APT, with 1 million ions collected before stopping data acquisition.

The tip was subsequently withdrawn and loaded into the electrolytic charging apparatus and charged with deuterium. Samples were immediately withdrawn from the charging apparatus and inserted into the atom probe, after first washing with D_2O , then isopropanol, and drying with an inert gas (Druckluft 40, DEKA). Samples were directly loaded into the atom probe, and then transferred through the vacuum system to the analysis chamber. A typical schedule for vacuum transfer is given in Table 1.

Experimental results

A Fe-30Mn-8Al-1.2C (wt.%) (Fe-26.8Mn-14.6Al-4.6C, at.%) sample was heat-treated at 600°C for 24 h to promote precipitation of secondary phase particles, namely κ -carbides [28]. APT mass-spectra for both the prior and post-charged states for a single tip were acquired. Pre and post-charged spectra for an Fe–Mn sample is shown in Fig. 3. The spectrum for the uncharged sample is randomly sampled from all reconstructed events in the uncharged state; this is done so that both spectra have the same total count (2.2×10^5 events – including uncharged events). This allows for direct comparison of amplitude – as evident from the near-identical background levels in the two measurements. As can be seen, there is an increase in the D:H ratio for the before and after charging experiments.

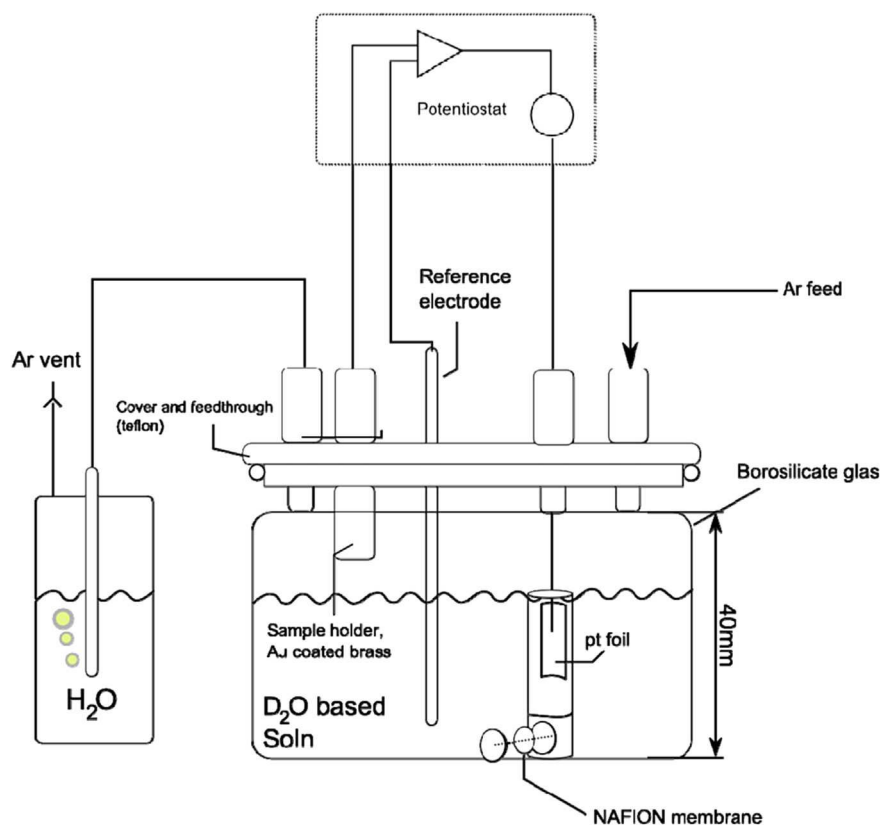


Fig. 1 – Schematic layout of deuterium charging apparatus, not to scale. Operating cell volume was $\sim 150 \text{ mL}$. Deuterium loading was conducted using a 0.1 M NaOD in D_2O solution for 1 h at -1.2 V .

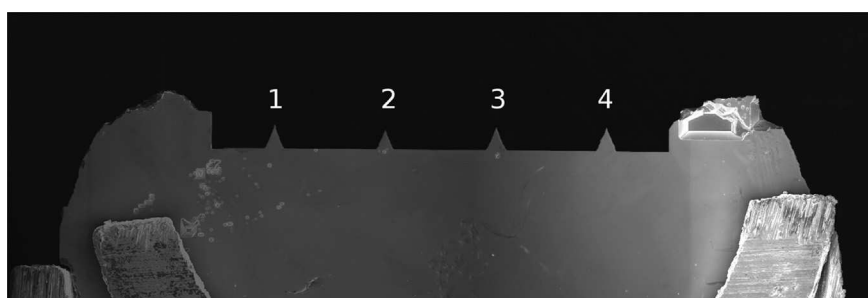


Fig. 2 – Example of sample geometry used in charging experiments. Substrate is silicon, and is mounted into the holder system of Herbig et al. [37].

Across $n = 16$ tips (1 M atoms each) in the uncharged state, a mean D:H ratio of 0.014 was found, with a standard deviation of 0.029. The low mean is only marginally perceptible from the background. This implies that a ratio of at minimum 0.071 is required to confirm successful charging for a single sample (95% confidence). For the charge shown in Fig. 3, in the uncharged state, the mass 2:1 ratio was 0.008, after D charging the ratio is increased to 0.16. Thus, given that $0.16 \gg 0.071$, it can be confirmed that the D:H ratio after charging is changed by the charging procedure to a statistically significant level – this corresponds to a significance level of >5 -sigma that the measurement is not simply a random fluctuation in the D:H ratio.

The atomic concentrations before and after charging are summarised in Table 2. Some contamination, presumably from the sample (Pt, Ga) or from either the cleaning solution or a carbide (CH, C₂), is evident after charging. Insufficient data was obtained from the run to determine if these contaminants decrease in concentration as a function of depth.

Despite the presence of a peak at mass-to-charge 2 after deuterium charging, which as previously discussed is statistically significant when compared to the uncharged state, it cannot be directly interpreted as successful deuterium loading from this experiment without additional supporting data. For instance the charging procedure, particularly in light of the changed sample concentration, could have altered the rate of formation of H₂ molecules. Subsequently, the experiment was repeated, using non-deuterated NaOH and H₂O under otherwise identical loading conditions as compared to deuterium loading. This is hereafter referred to as a null-charge.

For comparison between the non-deuterated experiment, across 3 successful runs, the maximal change in H₂:H ratio achieved in the null-charged state was an increase of factor 3.4 (from an initial 0.015 to a final 0.048). This compares with the deuterated solution, which had a maximal D:H ratio

change of 19.6 from the uncharged to charged state (0.008–0.16). This result indicates that the mass 2 peaks identified in the charged experiments are primarily deuterium, rather than a change in the molecular formation rates. As will be subsequently demonstrated (Fig. 4), for sufficiently long runs, the D:H ratio increases with increasing depth, suggesting that deuterium is contained within the sample, rather than purely at the surface.

To determine the time-dependence of the charging procedure, additional D₂O charging was performed, deliberately delaying the insertion of samples onto the cold-head. Samples were inserted after holding for 2 h, and the D:H ratio measured. Sample yield for these experiments (defined as >500 k measured ion events) was improved with 3 successful measurements from 8 as opposed to 1/8 from the 1 h transfer. The D:H ratios after charging were, averaged over these 3 experiments 0.021 with standard deviation $\sigma = 0.029$. These results suggest that the amplitude of the deuterium signal is indeed time dependant, as a statistically significant level of D was not reached for any sample charged and held at the 2 h time, when considering the significance threshold for the uncharged state ($0.021 \ll 0.071$).

As silver coated samples have shown to have improved yields [29], a charging experiment was conducted with a small

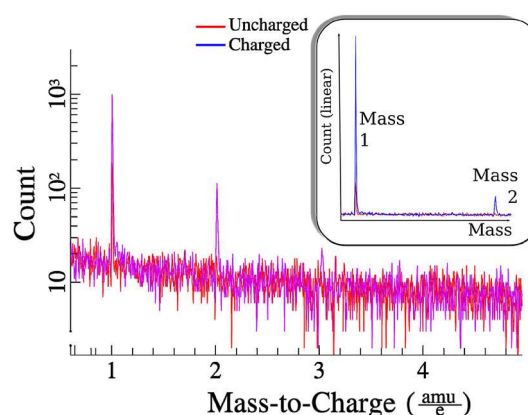


Fig. 3 – Low-mass region of mass spectrum before and after charging (~220 k ions). Mass 2:1 ratio before charging is 0.008, after charging the ratio is 0.16 (both values background corrected). Inset shows linear scaling of mass 1 and 2 peaks.

Table 1 – Typical transfer times from charging cell to APT, for each vacuum stage.

Stage	Time (Min)
Load lock in	2
High vacuum in	22
Cold head (UHV)	41

Table 2 – Measured species concentrations, before and after charging. Species marked as “-” were not present in the pre-charge case.

Species	Conc. (at.%), uncharged	Conc. (at.%), charged
C	4.2	8.0
Fe	57.5	29.4
Al	12.6	5.0
Mn	19.6	10.3
C ₂	1.2	1.3
H ₂ O	2.0	2.0
O	0.6	4.0
H	2.2	7.7
Pt	–	18.3
Ga	–	9.1
D	–	1.2
PtC	–	3.8

quantity of AgCl present in the solution. This allowed for the deposition of Ag onto the sample during charging. Further, it is known that Ag forms a low-permeability barrier due to its low hydrogen solubility and diffusivity at room temperatures [30] – the objective here being to trap D within the sample. Using this method, a sample was successfully run with a total data acquisition length of 4.5 M ions. The voltage curve (applied voltage to the sample vs. ion sequence) for this run was not smooth, but did not have any major jumps which would indicate sample fracture during APT. The silver layer was not removed prior to final sample fracture.

The composition of several species along the analysis direction are shown in Fig. 4, where it can be seen that the AgD concentration increases with increasing depth in the experiment, as compared to the AgH concentration. Indeed, there is a transition at ~50 nm in depth. The H and D concentration changes are more difficult to discern owing to the limited count. Contaminant species, such as Na⁺, Cl⁺, and NaCl⁺ decreased throughout the experiment (Fig. 4a). Most significant is the presence of small groupings of detected D-atoms, as shown in (Fig. 5). This is not accompanied by the presence of H, nor is there a local change in noise level near these areas. A simple comparison of cluster analyses, using the maximum separation method [31,32], ($d_{\max} = 0.5$, $N_{\min} = 3$), for the original and randomised datasets reveal that there are 40 clusters present for the original, and 8 clusters for the

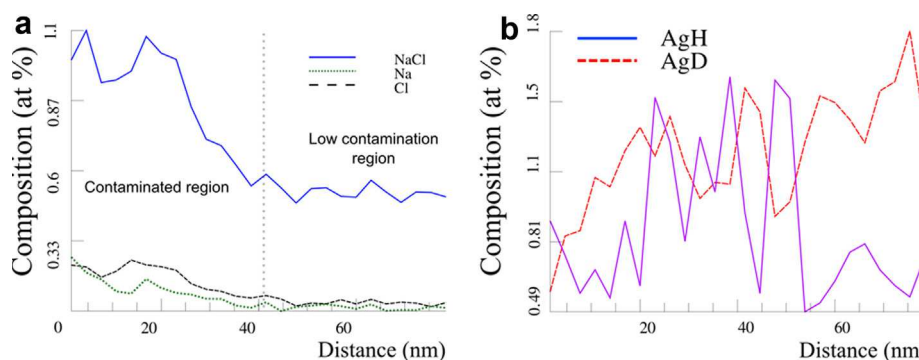


Fig. 4 – (a) Primary contaminant species as a function of depth for Ag coated material (b) AgH/AgD values as a function of depth. Contaminant species decrease, while the AgD:AgH ratio increases. Increasing distance in plot corresponds to increasing depth in sample.

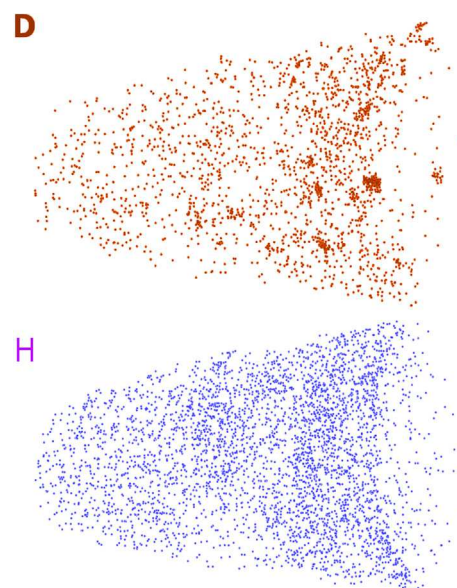


Fig. 5 – Comparison of Deuterium and Hydrogen distributions for Ag co-deposited sample, showing only the Ag layer. Deuterium and hydrogen distributions are clearly spatially differentiated.

randomised datasets, respectively (each random cluster having exactly 3 Deuterium atoms each). Here d_{\max} is the linking distance between atoms for cluster formation, and N_{\min} is the minimum number of ions allowed before a grouping of atoms is allowed to be designated as a cluster.

The randomisation of the dataset and cluster analysis was conducted in order to compare the number of hydrogen clusters identified in the experimentally obtained with the artificially randomized datasets. This allows for differentiation between cluster frequencies that are expected in the randomly distributed case, and those that are physically significant.

From the large difference in frequency between randomised datasets and the original, it is clear that the D atoms are not spatially random. Fig. 4 shows the distributions of H and D separately, clearly displaying the different spatial

distributions for the two species. Additional D atoms are present as AgD, but not shown in the 3D maps.

Some post-charge and post-APT investigation was conducted on charged samples (without Ag), to ascertain the quality of the charging surface and tip-shape, as shown in Fig. 6. Delamination of one of the Pt welds was evident, occurring during either the APT or charge stages. The tip itself had a relatively smooth appearance after charging (and subsequent APT for 20 k events), suggesting minimal re-deposited material during the charge.

Discussion

Utilising the theoretical solution for the diffusion of hydrogen from an infinite cylinder of $R = 100$ nm [33] and using macroscopic diffusion and austenitic solubility data of Farrel and Lewis [17], the concentration–diffusion rate for a small tip at room temperature was calculated to provide an estimate of transfer times required for retaining diffusible hydrogen.

As an atom probe tip provides additional free surfaces beyond that of an infinite cylinder, the solution should provide a lower bound to the true hydrogen content that exists in a tip with a zero degree shank and radius of 100 nm. Using this model, as given in Equation (1), and assuming that the APT has a detection threshold of ~ 1 ppm (more sensitive than realisable values), the hydrogen content of the cylinder drops rapidly to below detectable levels within 2 s. In this equation, J_0 and J_1 are the Bessel functions, α_n is the n th Bessel root, a is

the cylinder radius, $f(r)$ is the initial concentration field, D is diffusivity and t is time. The series was evaluated for the first 5 roots, using a value for D of 1.4 nm²/s.

$$C = \frac{2}{a^2} \sum_{n=1}^{\infty} \exp(-D\alpha_n^2 t) \frac{J_0(r\alpha_n)}{J_1^2 a \alpha_n} \int_0^a r f(r) J_0(r\alpha_n) dr \quad (1)$$

However, the experimental results contradict this prediction, showing detectable levels of D, for timescales of an hour after loading when operating at room temperatures. This would suggest two possible scenarios, either the macroscopic model is inapplicable at these scales, or the data for diffusion in austenite is inapplicable to the investigated material. There are several possible mechanisms that could explain the detectability of deuterium at time-scales of 1 h after charging. Potential mechanisms include hydrogen trapping to microstructural features, or limited accuracy of a pure diffusion model at this length scale, such as inaccurate diffusion constants due to lack of grain boundaries or the presence of surface barriers. It is assumed, for this work, that the primary cause of the mismatch between the experimental and theoretical diffusion result is due to the presence of a H-absorption/desorption barrier at the vacuum–specimen interface. A schematic diagram of a possible diffusive scenario that could perhaps model the observed results is given in Fig. 7, where Δt is the post-vacuum cryogenic time (ie time after charging completion).

Whilst a trapping mechanism is possible and cannot be excluded, the lack of clear spatial separation in this dataset precludes confirmation of trapping.

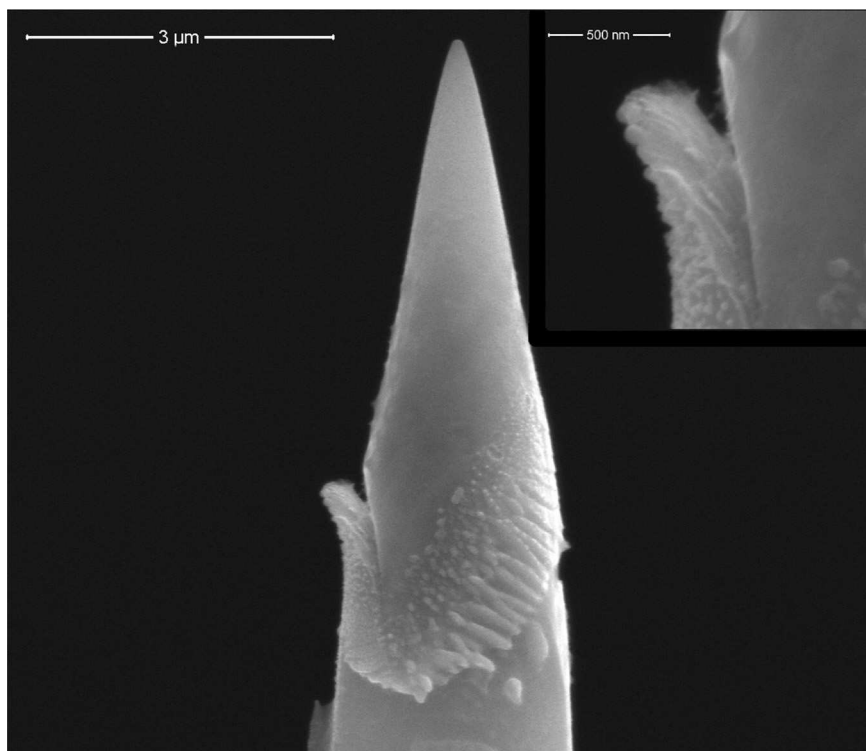


Fig. 6 – Sample after APT (1 M ions), D charging in a solution of D₂O + 0.1 M NaOD, w/o Ag and subsequent APT tip evaporation for 20,000 events. Inset shows close-up of Pt weld delamination.

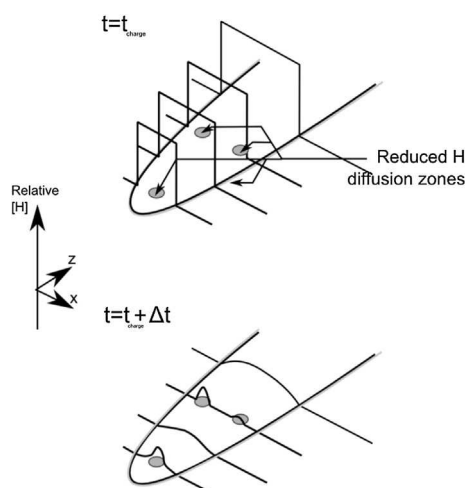


Fig. 7 – Schematic indicating possible diffusion process that would be consistent with atom probe observations. Regions of reduced diffusion rate would have a relatively increased hydrogen concentration, as observed in Ag dataset. Boundary at tip surface conditions imply continuous deuterium loss.

Due to the limited yield, i.e. the limited number of ions collected in these experiments prior to sample fracture, little information can be obtained regarding the 3D distribution of H within the Fe–Mn material. However, the spectral information (Fig. 3) can still be treated as valid. This is due to the null-charge experiment, which mitigate the concerns of H₂ formation being mistaken for D.

These results imply that the D concentrations measured (~1.2%), are unlikely to be artefacts, but rather are an underestimate for the true hydrogen content immediately after charging. The under-estimate is believed to originate from the inability to quench the sample sufficiently quickly due to vacuum transfer limitations, as evidenced by the delayed transfer experiments which yielded a substantially reduced D:H ratio. This underscores the need for investigation of cryogenic transfer methods in future experiments.

For the Ag co-deposited samples, the D content was significantly higher, (D:H ratio of 0.84), when using the D:H ratio as the primary metric, Figs. 4 and 5. The nature of the D clusters (Fig. 5) detected within the Ag coated sample are unclear, due to their limited count, and their unclear arrangement (not line or loop). Due to the decreasing (and highly depleted) concentration of contaminant species (e.g. Na) as a function of depth (Fig. 4a), it is surmised that the contamination layer is not responsible for these clusters. Despite the unclear origin of these D clusters, this result nevertheless shows that electrochemical charging methods can obtain usable quantities of APT data for location of hydrogen, under appropriate conditions.

Limitations and future work

The method is currently assumed to be restricted by the availability of deuterated species for charging, due to (to the

author's knowledge) limited data concerning the interaction of deuterated and non-deuterated species at the desired charging conditions. Specifically, whilst [OH⁻] and [D₂O] exchange data for the D ↔ H was found, only pH = 7 data was found [34], and this was interpreted as suggesting a slow reaction for D₂O, suggesting the use of an a-priori deuterated solvent to ensure the decomposition of NaOH in D₂O to Na⁺ and OD⁻. Using deuterated solvent eliminates concerns about inadvertent protium (H) charging when attempting to load D, but severely limits charging solution availability.

However, the main restriction in the imaging capability of this technique is the highly reduced sample yield after H charging. For several differing sample types (Several Fe–Mn samples, a Cu–V multilayer and an Ag coated sample) it was found that a total dataset length of no more than 2 M ions could be acquired across more than 18 attempted charging runs (1 h RT holding time).

Experimental yield is therefore a key limiting factor in the utility of this method. Whilst it is well known that laser atom probe can improve experimental yield, it also promotes molecular ion formation, which complicates the correct identification of deuterated material, thus limiting this route as a potential option for enhancing yield. Furthermore, the APT sample is heated up during laser pulsing to an unknown temperature, which can cause diffusion of deuterium atoms and lead to difficulties in determining their positions.

Future works may wish to consider how to improve the yield from APT experiments, such as via carefully controlled or calibrated capping layer deposition. Capping layers may aid in reducing the evaporative field and thus force on the sample [35]. It is conceivable that a low-field outer shell may provide mechanical strength, whilst allowing a smaller high-field core to evaporate, under steady-state conditions. Electropolished samples may prove more robust than their FIB prepared counterparts due to fewer problems with weld quality during the charge (Fig. 6). Work is currently underway to enable rapid transfer of electropolished samples into the APT after charging.

Some system considerations can further be used to improve these experiments. Utilisation of a straight-flight path instrument may aid in increasing total deuterium signal. Signal improvement would arise by increasing the pulse frequency (here 100 kHz, due to Ag peak, and potential Pt contamination) which is known to reduce the hydrogen signal arising from the chamber [36]. Such an alteration may require a straight-flight path system, as reflectron systems otherwise cause wrap-around for high-mass species (e.g. Ag/Pt) [38], due to their larger effective flight-path.

Conclusions

Electrolytic methods for charging hydrogen provide a viable alternative to deuterium charging via gas means. As shown here, it is possible to charge, detect in the mass spectra and image deuterium within a target sample, however, sample yields are limited.

Whilst further investigation is required to improve sample yield and deuterium signal, electrochemical methods significantly simplify the requirements for APT investigations of H

distributions in standard atom probe systems. Such a technique, if sufficiently improved from the perspective of sample yield, could provide a clear methodology for visualising and exploring hydrogen interaction to microstructural features, as demonstrated here.

Acknowledgements

The authors wish to acknowledge the assistance of Salzgitter Mannesmann Forschung GmbH, who provided funding for Dr Haley, and for project support under an industrial grant.

REFERENCES

- [1] Birnbaum HK, Sofronis P. Hydrogen-enhanced localized plasticity - a mechanism for hydrogen related fracture. *Mater Sci Eng* 1994;176:191–202.
- [2] Koyama M, Springer H, Merzlikin SV, Tsuzaki K, Akiyama E, Raabe D. Hydrogen embrittlement associated with strain localization in a precipitation-hardened FeMnAlC light weight austenitic steel. *Int J Hydrogen Energy* 18 March 2014;39(9):4634–46.
- [3] So KH, Kim JS, Chun YS, Park K-T, Lee Y-K, Lee CS. Hydrogen delayed fracture properties and internal hydrogen behavior of a Fe-18Mn-1.5Al-0.6C TWIP steel. *ISIJ Int* 2009;49:1952–9.
- [4] Park I-J, Jeong K-H, Jung J-G, Lee CS, Lee Y-K. The mechanism of enhanced resistance to the hydrogen delayed fracture in Al-added Fe-18Mn-0.6C twinning-induced plasticity steels. *Int J Hydrogen Energy* 2012;37:9925–32.
- [5] Dieudonné T, Marchetti L, Wery M, Miserque F, Tabarant M, Chène J, Allely C, Cugy P, Scott CP. Role of copper and aluminum on the corrosion behavior of austenitic Fe-Mn-C TWIP steels in aqueous solutions and the related hydrogen absorption. *Corros Sci* 2014;83:234–44. ISSN 0010-938X, <http://dx.doi.org/10.1016/j.corsci.2014.02.018>.
- [6] Han Do Kyeong, Kim Yong Min, Han Heung Nam, Bhadeshia HKDH, Suh Dong-Woo. Hydrogen and aluminium in high-manganese twinning-induced plasticity steel. *Scr Mater* June 2014;80:9–12. ISSN 1359-6462, <http://dx.doi.org/10.1016/j.scriptamat.2014.01.039>.
- [7] Ryu JH, Kim SK, Lee CS, Suh D-W, Bhadeshia HKDH. Effect of aluminium on hydrogen-induced fracture behaviour in austenitic Fe-Mn-C steel. *Proc Royal Soc Math Phys Eng Sci Royal Soc* 2012;469:20120458.
- [8] Ebihara K, Kaburaki H. Numerical modeling of thermal desorption spectra of hydrogen: a review of thermal desorption models. *ISIJ Int* 2012;52:181–6.
- [9] Daw MS, Baskes MI. Semiempirical, quantum mechanical calculation of hydrogen embrittlement in metals. *Phys Rev Lett* 1983;50:1285–8.
- [10] Evers S, Rohwerder M. The hydrogen electrode in the “dry”: a Kelvin probe approach to measuring hydrogen in metals. *Electrochem Commun* 2012;24:85–8.
- [11] Takahashi J, Kawakami K, Kobayashi Y, Tarui T. The first direct observation of hydrogen trapping sites in TiC precipitation-hardening steel through atom probe tomography. *Scr Mater* 2010;63:261–4.
- [12] Takahashi J, Kawakami K, Tarui T. Direct observation of hydrogen-trapping sites in vanadium carbide precipitation steel by atom probe tomography. *Scr Mater* 2012;67:213–6.
- [13] Gemma R, Al-Kassab T, Kirchheim R, Pundt A. Visualization of deuterium dead layer by atom probe tomography. *Scr Mater* 2012;67:903–6.
- [14] Karnesky RAJ, Bartel N, Huang D, Teslich N, Kumar M. Imaging and quantification of hydrogen isotope trapping. Sandia National Laboratories; 2012.
- [15] Takamizawa H, Hoshi K, Shimizu Y, Fumiko Yano KI, Nagata S, Shikama T, et al. Three-dimensional characterization of deuterium implanted in silicon using atom probe tomography. *Appl Phys Express* 2013;066602.
- [16] Takahashi J, Kawakami K, Ohmori H. Gas charge container, atom probe apparatus, and method for analyzing hydrogen position in material. United States patent application 20110113858.
- [17] Farrel, Lewis. The hydrogen content of austenite after cathodic charging. *Scr Met* 1981;15:661–4.
- [18] Song EJ, Suh D-W, Bhadeshia H. Theory for hydrogen desorption in ferritic steel. *Comput Mater Sci* 2013;79:36–44.
- [19] Li D, Gangloff RP, Scully JR. Hydrogen trap states in ultrahigh-strength AERMET 100 steel. *Metall Mater Trans* 2004;35:849–64.
- [20] Yamaguchi M, Ebihara K-I, Itakura M, Kadoyoshi T, Suzudo T, Kaburaki H. First-principles study on the grain boundary embrittlement of metals by solute segregation: part II. Metal (Fe, Al, Cu)-hydrogen (H). *Syst Metall Mater Trans* 2011;42:330–9.
- [21] Tien J, Thompson A, Bernstein IM, Richards RJ. Hydrogen transport by dislocations. *Metall trans A* 1976;7a:821–9.
- [22] Nagumo M. Function of hydrogen in embrittlement of high-strength. *Steels ISIJ Int* 2001;41:590–8.
- [23] Fukai Yuh, Ishii Y, Goto Yoshihiro, Watanabe K. Formation of superabundant vacancies in Pd-H alloys. *J Alloys Compd* 2000;313:121–32.
- [24] Ishikawa R, Okunishi E, Sawada H, Kondo Y, Hosokawa F, Abe E. Direct imaging of hydrogen-atom columns in a crystal by annular bright-field electron microscopy. *Nat Mater* 2011;10:278–81.
- [25] Pundt A, Kirchheim R. Hydrogen in metals: microstructural aspects, annual review of materials research. *Annu Rev* 2006;36:555–608.
- [26] Kellogg GL. Pulsed-laser atom probe mass spectroscopy. *J Phys Sci Instrum* 1987;20:125–36.
- [27] Andreev BM, Zel'venskii YaD, Uborskii VV. Distribution of tritium between liquid and gas in the case of isotope equilibrium in water-hydrogen sulfide and heavy water-sulfur deuteride systems. *Sov At Energy* 1978;44(3):266–71. <http://dx.doi.org/10.1007/BF01117633>.
- [28] Gutierrez-Urrutia I, Raabe D. Influence of Al content and precipitation state on the mechanical behavior of austenitic high-Mn low-density steels. *Scr Mater* 2013;68:343–7.
- [29] Larson DJ, Prosa T, Bunton JH, Lawrence D, Oltman E, Strennen S, et al. Improved mass resolving power and yield in atom probe tomography. *Microsc Microanal* 2013;19:994–5.
- [30] Zvezdin Y, Belyakov Y. Hydrogen permeability of some transition metals and metals of group I of the periodic system. *Mater Sci* 1967;255–6.
- [31] Stephenson LT, Moody MP, Liddicoat PV, Ringer SP. New techniques for the analysis of fine-scaled clustering phenomena within atom probe tomography (APT) data. *Microsc Microanal* 2007;13:448–63.
- [32] Vaumousse D, Cerezo A, Warren P. A procedure for quantification of precipitates microstructures from three-dimensional atom probe data. *Ultramicroscopy* 2003;95:215–21.
- [33] Crank J. The mathematics of diffusion. Clarendon Press; 1975.
- [34] Natzle WC, Bradley Moore C. Recombination of H+ and OH- in pure liquid water. *J Phys Chem* 1985;89:2605–12.

-
- [35] Moy CK, Ranzi G, Petersen TC, Ringer SP. Macroscopic electrical field distribution and field-induced surface stresses of needle-shaped field emitters. *Ultramicroscopy* 2011;111:397–404.
- [36] Sundell G, Thuvander M, Andrén H-O. Hydrogen analysis in APT: methods to control adsorption and dissociation of H₂. *Ultramicroscopy* 2013;132:285–9.
- [37] Herbig M, Raabe D, Li YJ, Choi P, Zaefferer S, Goto S. Atomic-scale quantification of grain boundary segregation in nanocrystalline material. *Phys Rev Lett* 27 March 2014;112:126103.
- [38] Larson DJ, Prosa TJ, Ulfing RM, Geiser BP, Kelly TF. Local electrode atom probe tomography: a user's guide. Springer; 2013.
- [39] Reichenbach B, Solanoand I, Schwoebel PR. A field evaporation deuterium ion source for neutron generators. *J Appl Phys* 2008;103:094912.